Joint Diseases and Related Surgery

Jt Dis Relat Surg
2026;37(3):851-862

ORIGINAL ARTICLE

The influence of design factors on the mechanical properties of biodegradable composite plates: A finite element analysis

Mustafa Buğra Ayaz, MD[1], Ali Çağrı Tekin, MD[2], Süreyya Ergün Bozdağ, PhD[3], Serhat Gürbüz, MD[1], Mehmet Kürşad Bayraktar, MD[2], Esra Akdaş Tekin, MD[4]

[1]Department of Orthopedics and Traumatology, Metin Sabancı Baltalimanı Bone Diseases Training and Research Hospital, İstanbul, Türkiye
[2]Department of Orthopedics and Traumatology, Prof. Dr. Cemil Taşcıoğlu City Hospital, İstanbul, Türkiye
[3]İstanbul Technical University, Faculty of Mechanical Engineering, Laboratory of Biomechanics and Strength of Materials, İstanbul, Türkiye
[4]Department of Anesthesiology and Reanimation, Prof. Dr. Cemil Taşcıoğlu City Hospital, İstanbul, Türkiye

The mechanical properties of an orthopedic implant are influenced by a wide range of parameters, including the implant material, fixation method, positioning, and screw application configuration.[1] Through proper design, mechanically superior implants can be produced using less material. Furthermore, changes in the implant's microarchitectural configuration can significantly alter the loading patterns and its response to stress. Therefore, advanced evaluation methods such as finite element analysis (FEA) are required to investigate the biomechanical properties of anisotropic composite materials and implants of varying geometries.[2]

Received: June 22, 2026
Accepted: July 15, 2026
Published online: July 23, 2026

Correspondence: Mustafa Buğra Ayaz, MD. Metin Sabancı Baltalimanı Kemik Hastalıkları Eğitim ve Araştırma Hastanesi, Ortopedi ve Travmatoloji Kliniği, 34470 Sarıyer, İstanbul, Türkiye.

E-mail: bugrayaz@gmail.com

Citation: Ayaz MB, Tekin AÇ, Bozdağ SE, Gürbüz S, Bayraktar MK, Tekin EA. The influence of design factors on the mechanical properties of biodegradable composite plates: A finite element analysis. Jt Dis Relat Surg 2026;37(3):851-862. doi: 10.52312/jdrs.2026.3004.

© 2026 Joint Diseases and Related Surgery. This is an open access article published under the terms of the Creative Commons Attribution-NonCommercial 4.0 International License (CC BY-NC 4.0), which permits non-commercial use, distribution, reproduction, and adaptation in any medium, provided the original work is properly cited. http://creativecommons.org/licenses/by-nc/4.0/

ABSTRACT

Objectives: This study aims to investigate the influence of implant design factors on mechanical behavior and to identify lower-profile biocomposite plate configurations with mechanical responses approaching those of a titanium reference construct under selected loading conditions.

Materials and methods: In this computational finite element study, three-dimensional implant models were developed, and material properties of polyamide-6/nano-hydroxyapatite and titanium alloy (Ti6Al4V) were assigned. Seven composite plate types were modeled: flat (thicknesses 8, 9, and 10 mm), bellied, curved, enhanced, and hybrid plate. All constructs were mounted on a cylindrical synthetic femoral diaphyseal surrogate and fixed with six screws. Finite element analysis was conducted using ANSYS Mechanical 2022 R2 under axial compression (800 N), distraction (300 N), and torsion (10 Nm). Mechanical responses including maximum deformation, von Mises stress, and strain distribution in bone, plate, and screws were evaluated. Results were evaluated descriptively and comparatively across implant configurations and loading conditions.

Results: The titanium construct generally demonstrated the lowest deformation under torsional loading and the lowest plate strain response, whereas selected composite geometries approached or exceeded titanium-like deformation performance under specific loading modes. The hybrid plate showed the lowest deformation under compression, while the thick flat plate provided the lowest deformation among composites under distraction and torsion. The bellied design showed lower torsion-induced deformation and lower plate stress than most other lower-profile composite configurations. The enhanced plate exhibited the lowest plate strain among the composite models under compression and distraction but may pose challenges for soft tissue coverage due to its complex geometry.

Conclusion: Optimizing plate geometry can substantially modify the mechanical behavior of biodegradable composite constructs. Hybrid and enhanced designs demonstrated load-mode specific mechanical responses that may inform future biodegradable plate optimization, particularly with further material refinement and experimental validation.

Keywords: Biodegradable plate, biomechanics, composite material, finite element analysis, fracture fixation, implant design

Stress distribution in both the bone and the implant is crucial for successful fracture healing. However, excessive stress may increase the risk of implant failure and nonunion.[3] Among the most commonly used fixation devices in fracture repair are locking plates. The limited contact dynamic compression plate (LC-DCP) remains one of the most widely used and effective systems in contemporary orthopedic practice.[4] These plates provide fracture fixation under both absolute and relative stability principles. Less rigid fixation systems that allow for controlled micromotion are employed in selected cases aiming for secondary bone healing. In contrast, excessively rigid fixation may result in stress shielding, leading to increased bone porosity, delayed union, or even refractures.[5]

Stress shielding occurs when a rigid implant carries most of the physiological load, eliminating typical stress on the surrounding bone. Consequently, removal of osteosynthesis implants, particularly from diaphyseal bones, may result in secondary fractures. This stress shielding effect can be mitigated by adjusting the rigidity of the implant material or minimizing the strain mismatch between the implant and the bone tissue.[6] Two key mechanical descriptors after fracture fixation are axial rigidity (EA) and flexural rigidity (EI). Axial rigidity reflects the load displacement response under axial compression and is determined by the material's Young's modulus (E) and the cross-sectional area (A). Flexural rigidity characterizes resistance to deformation when indirectly loaded and depends on the material modulus (E) and the second moment of area of the cross-section (I). Both parameters are influenced by the material's mechanical properties and cross-sectional configuration.[7]

Biocomposite materials offer characteristic biological properties such as biodegradability, drug-loading capacity, and bioconductivity. As such, they play a key role in numerous applications in tissue engineering, including fracture stabilization, defect reconstruction, infection prevention, and malignancy control.[8] Biodegradable implants, by dissolving *in vivo*, reduce the need for implant removal and lower the risk of infection. When composed of polymers and ceramics, biodegradable composite implants mimic the mechanical properties of bone, reduce stress shielding, and support healthy bone development, particularly in pediatric patients.[9] Despite their sophisticated biological advantages, current biocomposite implants generally need to be manufactured with larger dimensions to achieve mechanical performance comparable to metallic implants. Nevertheless, in addition to material type and size, implant design is one of the most critical factors affecting mechanical behavior.

In this study, the aim was to investigate the design-related geometric parameters, including plate thickness, width, cross-section, and screw diameter, required for a biocomposite implant to approach titanium-like construct rigidity. As a biocomposite material, PA6-nHA was selected due to its partial resorbability, extensive preliminary characterization, and relatively strong mechanical performance compared to other degradable composite materials.[10] Previous finite element studies have evaluated biodegradable fixation plates and configuration factors; however, limited attention has been given to how distinct geometric plate modifications within the same composite material system alter construct-level responses under multiple loading modes.[11] The relative contribution of distinct geometric design features within the same composite material system has not been sufficiently clarified under different loading modes. Therefore, a comparative evaluation of distinct plate geometries under compression, distraction, and torsion may provide useful early-stage information for biodegradable plate design optimization.

MATERIALS AND METHODS

Material properties and model design

The finite element models consisted of three main material groups: a titanium alloy for the metallic reference plate and screws, PA6-nHA for the composite plates and screws, and a synthetic cylindrical structure representing the cortical bone analogue. The metallic plate was modeled using Ti-6Al-4V ELI (Grade 5), with elastic properties defined in accordance with ISO 5832-3 and ASTM (American Society for Testing and Materials) F136 specifications.[12] For the composite implants, polyamide-6 reinforced with 10 wt.% nano-hydroxyapatite (PA6-nHA) was adopted, with material properties taken from validated literature sources.[13] The bone surrogate was defined using fourth-generation Sawbones® (Pacific Research Laboratories, Inc., Vashon, WA, USA) cortical analogue properties as reported in manufacturer documentation and peer-reviewed summaries.[14] All materials were implemented as linear, elastic, and isotropic, and their parameters were compiled into a material card for direct use in the finite element environment (Table I). Informed consent was not required because this computational FEA did not

TABLE I
Mechanical characterization of materials used in the analysis

	Ti6Al4V[12]	PA6-nHA[13]	Bone model[14]
Ultimate tensile strength (MPa)	930	75.4	90
Young modulus (GPa)	116	3.52	12.4
Poisson ratio	0.33	0.3	0.26

Ti6Al4V, titanium alloy; PA6-nHA, polyamide-6/nano-hydroxyapatite.

involve human participants or identifiable patient data. The study protocol was approved by the Prof. Dr. Cemil Taşcıoğlu City Hospital Ethics Committee (Date: 01.07.2021, Approval No.: E-48670771-514.10). The study was conducted in accordance with the principles of the Declaration of Helsinki.

Although four-point bending is the standard bench method for characterizing bone plates and primarily evaluates their bending/compressive behavior, it does not fully capture construct behavior under different loading modes. In the present study, implant performance was assessed indirectly within an integrated fracture fixation system under compression, distraction, and torsion, allowing comparative evaluation of construct-level behavior across multiple loading modes. The three-dimensional (3D) analysis models were constructed comprising a cylindrical bone, a metallic plate with locking screws, and counterpart composite plates with locking screws. For the synthetic bone model, a cylinder measuring 300 mm in length and 30 mm in diameter with a cortical thickness of 7 mm was created to represent human femoral diaphysis. Then a transverse osteotomy with a 1-mm gap was made at the midshaft to simulate nondisplaced fracture. In all the fracture models, fixation was performed using six screws, skipping one hole each, and the plate bone distance was limited to ≤ 2 mm. The metallic reference plate was modeled according to ASTM F382 criteria and established DCP/LC-DCP design principles, including standardized plate dimensions and combined-hole geometry.[15,16] The titanium screw geometry followed ASTM F543 criteria; however, to reduce computational cost and focus on global construct behavior, screws were simplified to a smooth solid form without thread or other accessory features.[17] For the same reason, the LC-DCP undersurface grooves were omitted although the combi-hole architecture was retained to keep the model compatible with potential subsequent biomechanical testing studies.

The same overall geometric configuration (plate length, hole count/pitch, screw layout, and plate bone distance) but varied dimensions was applied across the composite constructs to enable direct comparison with the metallic reference. Given the material properties and the distinct architecture of the composite plates, the AO/ASIF (Association for the Study of Internal Fixation) fixation techniques such as dynamic compression, buttress, or bridging functions characteristic of metallic DCP/LCP systems are not expected to be reproduced.[4] Accordingly, the metallic reference was modeled with DCP characteristics, whereas the composite designs adopted a locking plate configuration appropriate to their intended use. These assemblies formed the basis for the finite element analyses used to evaluate construct responses under the specified loading conditions.

Design specifications and features of variant composite models

Three-dimensional models of the titanium and the composite implants and the cylindrical bone surrogate were created in SolidWorks Premium 2021 SP4.1 (Dassault Systèmes, Waltham, MA, USA). In accordance with ASTM F382, the metallic DCP plate was modeled as 152 mm in length, 10 mm in width, and 3 mm in thickness, with an inferior arc radius (R = 10 mm), blended with corner fillets (R = 1 mm), reproducing the typical crescent-type cross-section. Ten combi holes were spaced at a 12.5-mm pitch, with nominal diameters of 3.5 to 4.0 mm to accommodate 3.5-mm cortex screws.[15] Titanium screws conformed to ASTM F543 specifications, with a 3.0-mm shank and a nominal 3.5-mm head/seat diameter.[17]

For the composite implants, both the plate and the locking screw were initially modeled with equivalent configuration to the titanium standard to determine baseline mechanical performance. Composite plate sizing against the titanium reference was then performed by matching EI. Using literature moduli (PA6-nHA: 3.52 GPa; Ti-6Al-4V: 116 GPa),

the required composite cross sectional dimensions were obtained from EI = E × I so that the composite plate matched the titanium plate's EI.[12,13] Here, 'E' is Young's modulus and 'I' is the second moment of area (area moment of inertia) about the bending axis; for flat rectangular plate sections $I = (w \times t^3) \div 12$ (width: w, thickness: t). For screw shanks modeled as solid circular sections, I was calculated as $I = (\pi \times d^4) \div 64$ (diameter: d).[7] This scaling yielded a target thickness of approximately 8.5 mm for a 16-mm width at equal length. Accordingly, three flat composite plates were modeled at 8-, 9-, and 10-mm thickness (all 16-mm wide, 152-mm long) with an inferior arc radius of 15 mm, and corner fillets (R = 3.5 mm superior, R = 2.0 mm inferior), with 10 conical holes (tapering 9 to 8 mm) to receive composite screws. Composite screw diameter was likewise determined by EI matching to the 3.0-mm titanium shank, yielding a target of approximately 7-mm. In the models, a 7.5-mm cylindrical shank with an 8- to 9-mm conical head was used to engage the conical plate holes.

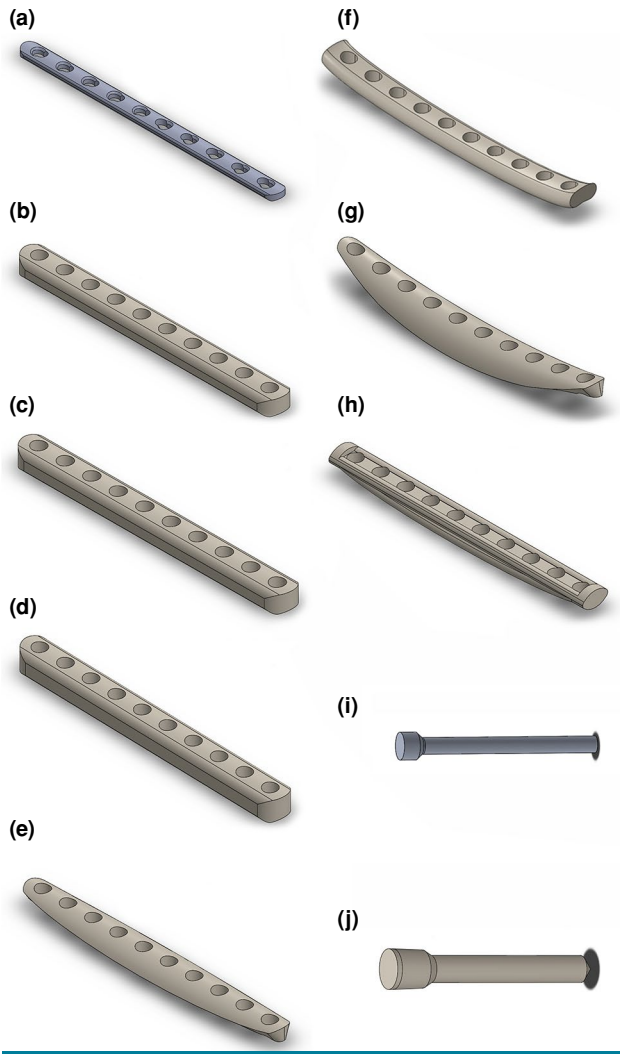


FIGURE 1. Design features of study models. **(a)** Ti6Al4V plate; **(b)** Slim flat plate; **(c)** Regular flat plate; **(d)** Thick flat plate; **(e)** Bellied plate; **(f)** Curved plate; **(g)** Enhanced plate; **(h)** Hybrid plate; **(i)** Ti6Al4V screw; **(j)** Composite screw.
Ti6Al4V, titanium alloy.

Additionally, alternative designs were generated by applying controlled, single-parameter modifications to the flat baseline. Plate length, hole pattern, screw positions, and plate bone distance were kept constant. The bellied plate was created by increasing mid span thickness with tapered transitions into the terminal segments. In terms of its overall design features, the bellied plate closely resembles Lambotte's plate (1909) in many respects.[16] The curved plate was generated by imposing a predefined sagittal curvature angle of 140° along the longitudinal axis; terminal regions were smoothly blended using tapered transitions. The curved plate design in the present study is similar in concept to the plate designs evaluated by Chandra et al.[11] in their study on Mg plates. The enhanced design combined the belly and curvature adjustments within the same parameter ranges. The hybrid model, derived from the flat and curved designs, combined a locally thickened central segment with a curved sagittal profile while maintaining flat terminal limbs. This resulted in the creation of seven composite plate models of varying geometries and thicknesses: flat (8, 9, and 10 mm), bellied (8 mm), curved (8 mm), enhanced (7 mm), and hybrid (7.5 mm) plates (Figure 1).

Model verification

Model verification was performed before comparative assessment of the composite configurations. Calculation verification included unit consistency checks, comparison of applied loads and moments with corresponding reaction forces and moments, and confirmation of global equilibrium for each load case. Solver convergence was monitored using the default ANSYS Mechanical (Ansys, Inc., Canonsburg, PA, USA) convergence criteria, and no unconverged load steps were accepted for postprocessing. Mesh convergence testing was conducted by refining mesh density until changes in maximum cortical bone stress and implant-bone interface micromotion were below 3%.[18]

The Ti6Al4V reference plate was then evaluated using independent benchmark simulations. In the ASTM F382-like four-point bending analysis, the

TABLE II
Implant thicknesses and dimensions

Implant type	Thickness (mm)	Volume (cm^3)	Node	Element
Ti6Al4V plate	3	3.5	54134	34203
Slim flat plate	8	15.3	97426	64734
Regular flat plate	9	17.2	104760	69736
Thick flat plate	10	21.5	130310	87535
Bellied plate	8	14.3	69632	45621
Curved plate	8	14.2	60569	39524
Enhanced plate	7	17.6	74135	48493
Hybrid plate	7.5	13.3	75975	50121
Ti6Al4V screw	3	0.3	38860	8686
Composite screw	7.5	1	23299-30939	14705-19758
4th Gen Sawbone®	7	149.5	128492-195580	86380-134164

Ti6Al4V, titanium alloy.

reference plate demonstrated a bending stiffness of 584.3 N/mm and a bending structural stiffness of 3.04 Nm^2, which was within the range of EI values previously reported for bone plates.[7] The peak von Mises stress under four-point bending was 235.06 MPa, remaining within the elastic range of Ti6Al4V. Together with the equilibrium and mesh convergence checks, these findings supported the numerical consistency of the reference plate geometry, material assignment, and bending boundary-condition implementation before applying the same computational framework to the comparative construct analyses.

Finite element analysis: loads and boundary conditions

Finite element analysis was performed in ANSYS 2022 R2 (Ansys, Inc., Canonsburg, PA, USA) using 10-node second-order tetrahedral elements (SOLID187). All materials were assumed homogeneous, linear elastic, and isotropic, whereas geometric nonlinearity was enabled to account for large deformation effects under the applied multiaxial loading. Plates, screws, and the cylindrical bone segment were meshed as fully integrated 3D volumes. A structured meshing strategy was used, with a target element size of approximately 0.2 to 1.0 mm for plates and screws and 1.0 to 1.5 mm for cortical and trabecular bone. Local refinements were applied around screw holes, the osteotomy line, and contact interfaces. Node and element counts ranged from 50,000 to 130,000 depending on the complexity of the implant configuration (Table II). Mesh quality was assessed using standard element quality metrics, including aspect ratio, skewness, and Jacobian ratio. Regions with potential numerical singularities at sharp contact transitions were interpreted cautiously, and

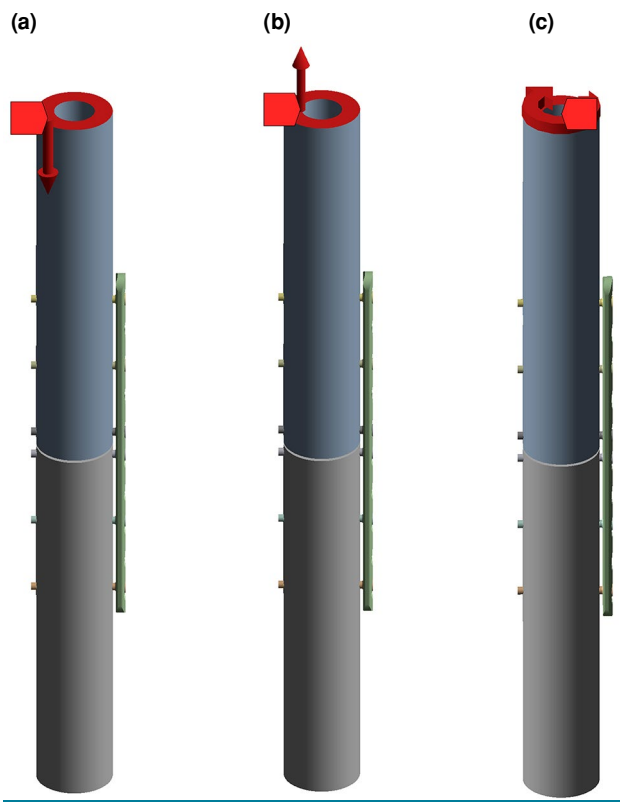


FIGURE 2. Loading conditions applied to fracture fixation models. **(a)** Compression (800N). **(b)** Distraction (300N). **(c)** Torsion (10 Nm).

comparative conclusions were based on consistent regions of interest across all models rather than isolated nodal peak values.

Implant-bone interfaces were defined as frictional contacts with a coefficient of friction of 0.64, representing a mechanically stable bone-implant contact scenario, while plate-screw interfaces were modelled as bonded to represent locked hardware integration.[19,20] The osteotomy gap between the proximal and distal bone segments was also modelled with a frictional bone to bone contact, allowing relative sliding and load transfer across the fracture plane.

For all simulations, a fixed support was applied over the entire distal circular surface of the cylindrical bone, constraining all translational and rotational degrees of freedom. The compressive load of 800 N was selected to provide a standardized axial loading condition comparable to previously reported biomechanical testing protocols using composite femoral models.[21] The distractive load of 300 N was used as a lower-magnitude comparative axial loading condition to evaluate construct response under tensile separation across the osteotomy. The torsional moment of 10 Nm was selected as a standardized comparative torsional load, consistent with previously reported finite element and biomechanical modelling approaches for plated femoral constructs.[19] These load cases were used as standardized unfavorable loading conditions that may be relevant when postoperative weight-bearing restrictions are insufficiently followed, rather than as a complete representation of routine postoperative physiological loading (Figure 2).

RESULTS

Across all loading conditions (compression, distraction, and torsion), total deformation (mm), maximum equivalent (von Mises) stress (MPa), and maximum equivalent strain (%) were evaluated for each plate-bone construct. Mechanical responses were interpreted according to load-mode specific endpoints, including total deformation, peak implant stress, screw stress, and equivalent strain distribution.

Deformation of plate-bone constructs

Total deformation varied according to both loading mode and implant geometry. Under compression, the hybrid composite plate showed the lowest construct deformation (14.8 mm), followed by the thick flat plate (16.0 mm) and the Ti6Al4V construct (18.5 mm). The enhanced plate also demonstrated a relatively low deformation response under compression (19.2 mm), whereas the curved and slim flat designs showed the highest compression-induced deformation values. Under distraction, the thick flat plate exhibited the lowest deformation (6.0 mm), closely followed by the Ti6Al4V construct (6.7 mm) and the enhanced plate (7.2 mm). The regular flat, hybrid, bellied, slim flat, and curved designs showed progressively higher distraction-induced deformation.

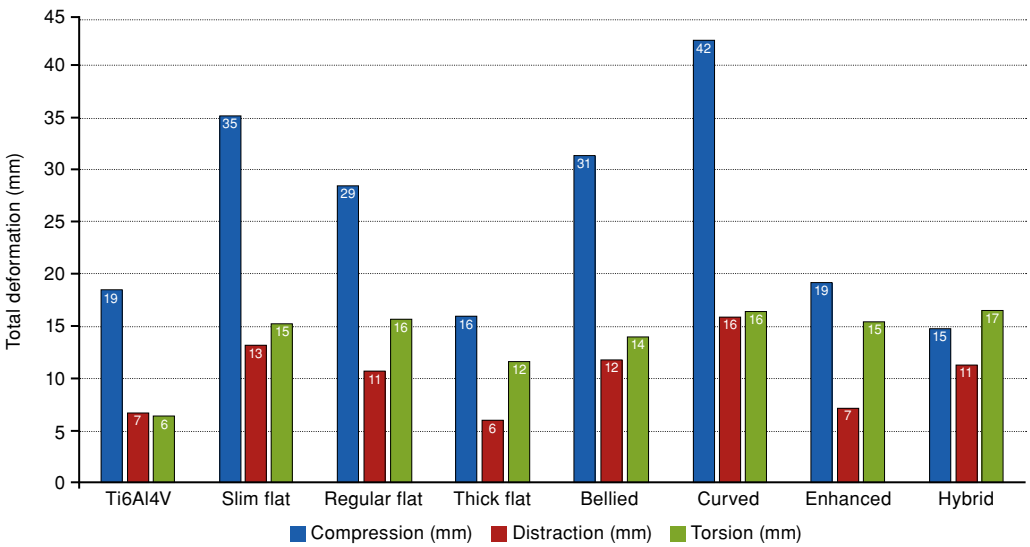


FIGURE 3. Total deformation on system under compression, distraction, and torsional loading.
Ti6Al4V, titanium alloy.

Under torsional loading, the Ti6Al4V construct showed the lowest total deformation (6.4 mm). Among the composite configurations, the thick flat plate demonstrated the lowest torsion-induced deformation (11.7 mm), followed by the bellied design (14 mm). The curved and hybrid models exhibited the highest torsion-induced deformation values among the composite constructs (Figure 3).

Stress distribution in plates, screws, and bone

Because plasticity, damage, and failure criteria were not included, peak von Mises stress values were interpreted as comparative indicators of stress concentration and load transfer rather than as definitive implant failure thresholds. Under compression, the Ti6Al4V construct showed the highest implant stress, with peak values of 1179 MPa in the plate and 1202 MPa in the screws. All composite configurations reduced implant stress compared to the metallic reference. The greatest reduction was observed in the hybrid model, with plate and screw stresses decreased by approximately 94% and 91%, respectively. The enhanced model showed the second lowest implant stress under compression, whereas the curved design demonstrated the highest plate and screw stresses among the composite constructs (Figure 4). Under distraction, the Ti6Al4V construct again demonstrated the highest implant stress. Among the composite configurations, the enhanced model showed the lowest plate and screw stresses, corresponding to reductions of approximately 93% and 95% compared to the metallic reference. The regular and thick flat models also maintained low stress levels under distraction, while the curved and hybrid designs showed relatively higher plate stresses among the composite constructs (Figure 5). Under torsional loading, the Ti6Al4V construct showed the highest plate and screw stresses. Among the composite configurations, the bellied and curved designs showed the lowest plate stresses, with reductions of approximately 85% and 84% relative to the metallic reference. However, the curved model did not show a comparable reduction in screw stress. The thick flat plate demonstrated the lowest screw stress under torsion, with an approximately 56% reduction compared to the Ti6Al4V construct. Overall, the hybrid and enhanced models showed the lowest implant stress under compression and distraction, whereas the thick flat and bellied designs exhibited lower combined deformation, plate stress, and screw stress response under torsional loading (Figures 6, 7).

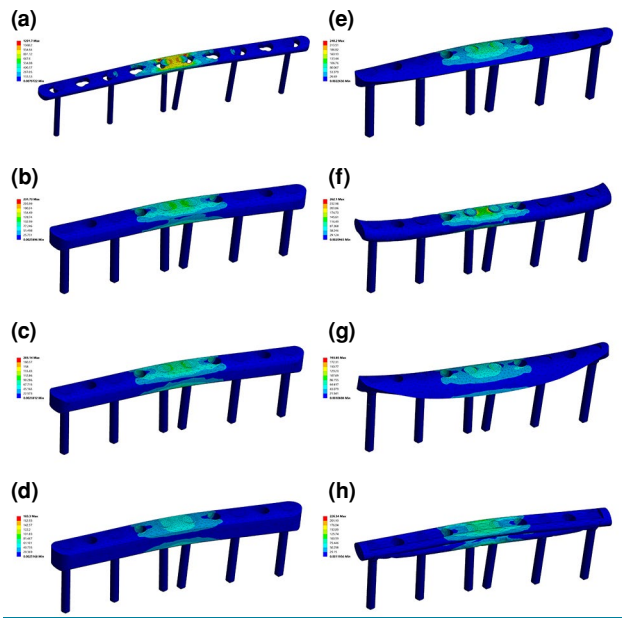


FIGURE 4. Stress distribution under compression loading. Peak von Mises stress values (MPa) are shown for each construct. **(a)** Ti6Al4V plate; **(b)** Slim flat plate; **(c)** Regular flat plate; **(d)** Thick flat plate; **(e)** Bellied plate; **(f)** Curved plate; **(g)** Enhanced plate; **(h)** Hybrid plate.
Ti6Al4V, titanium alloy.

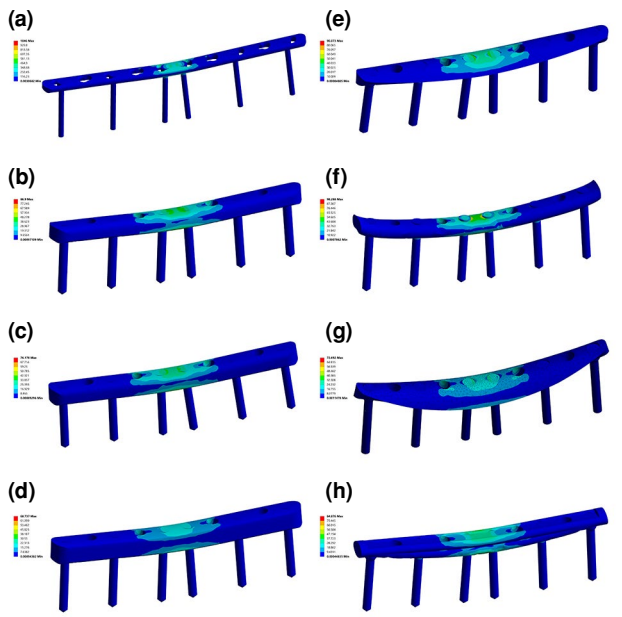


FIGURE 5. Stress distribution under distraction loading. Peak von Mises stress values (MPa) are shown for each construct. **(a)** Ti6Al4V plate; **(b)** Slim flat plate; **(c)** Regular flat plate; **(d)** Thick flat plate; **(e)** Bellied plate; **(f)** Curved plate; **(g)** Enhanced plate; **(h)** Hybrid plate.
Ti6Al4V, titanium alloy.

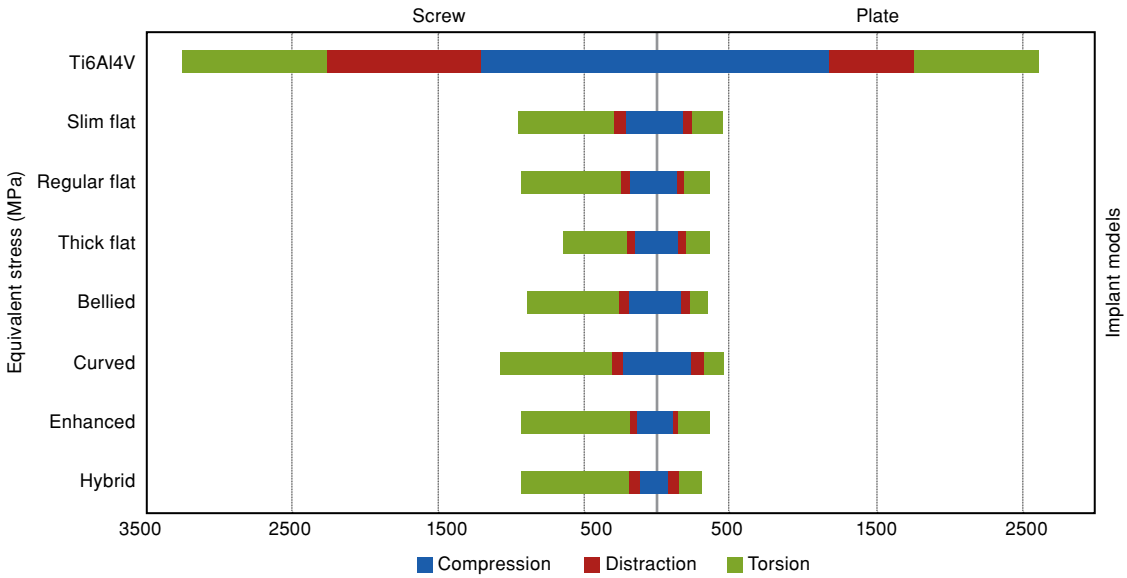


FIGURE 6. Maximum equivalent (von Mises) stress on plate and screw under compression, distraction, and torsional loading.
Ti6Al4V, titanium alloy.

Strain evaluation

Equivalent strain patterns differed according to implant material, geometry, and loading mode. The Ti6Al4V construct generally demonstrated lower plate strain than the composite configurations, consistent with its higher stiffness. Among the composite models, the enhanced plate showed the lowest plate strain under compression and distraction, whereas the hybrid, curved, and slim flat designs demonstrated comparatively higher strain values under compression.

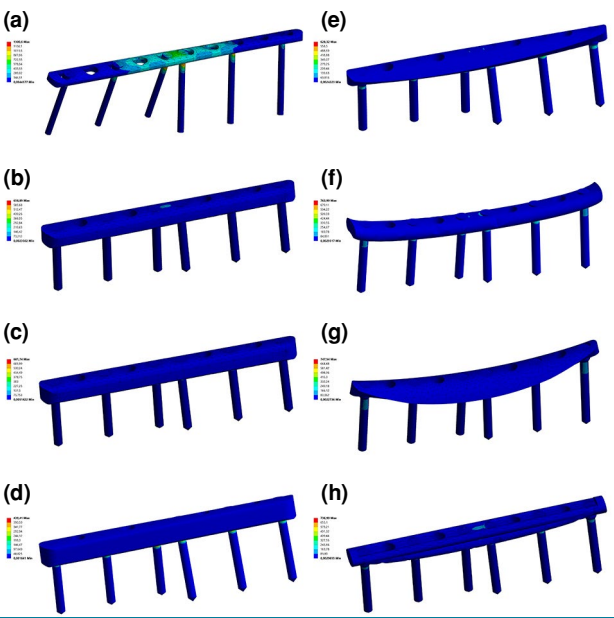


FIGURE 7. Stress distribution under torsional loading. Peak von Mises stress values (MPa) are shown for each construct. **(a)** Ti6Al4V plate; **(b)** Slim flat plate; **(c)** Regular flat plate; **(d)** Thick flat plate; **(e)** Bellied plate; **(f)** Curved plate; **(g)** Enhanced plate; **(h)** Hybrid plate.
Ti6Al4V, titanium alloy.

Under distraction, the enhanced, bellied, and thick flat plates showed relatively lower plate strain among the composite configurations, while the hybrid and curved designs exhibited higher values. Under torsional loading, the bellied and curved plates demonstrated the lowest plate strain among the composite models, followed by the thick flat and hybrid configurations. Bone strain varied across loading conditions and did not consistently follow the same pattern as plate strain. Overall, the enhanced model showed the lowest plate strain among the composite constructs under compression and distraction, whereas the bellied plate showed lower torsional plate strain and the thick flat plate showed lower torsional bone strain among the composite configurations (Figure 8).

DISCUSSION

In the treatment of long bone fractures, the mechanical environment is a critical determinant of healing prognosis. Current research supports that optimizing construct rigidity, either through appropriate implant selection or fixation technique,

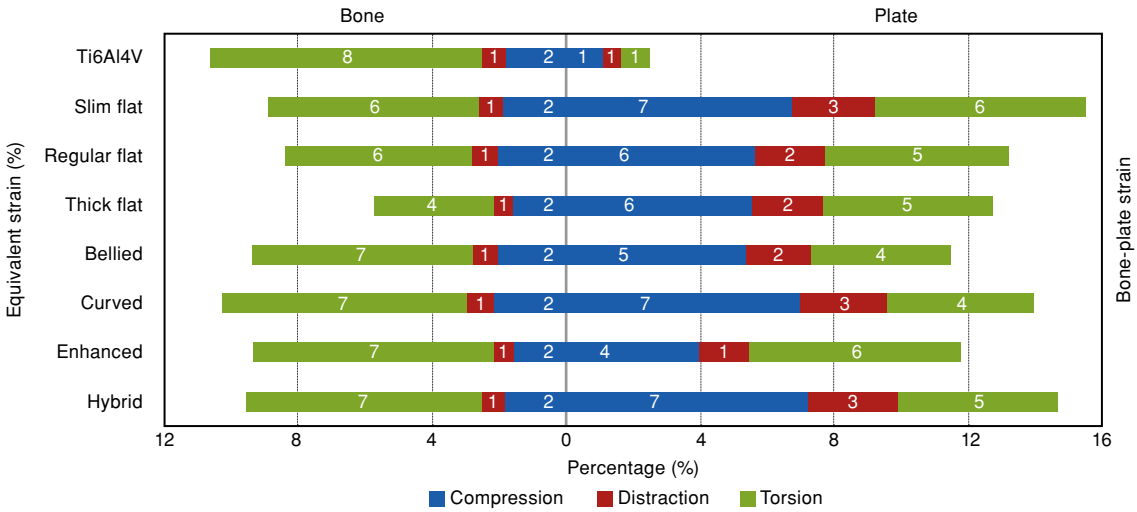


FIGURE 8. Maximum equivalent (von Mises) strain on plate and bone under compression, distraction, and torsional loading.
Ti6Al4V, titanium alloy.

results in more predictable clinical outcomes.[8] These outcomes are affected by both the intrinsic quality of the bone and the stage of healing. Aging and osteoporosis reduce cortical bone rigidity while paradoxically increasing trabecular rigidity. Moreover, reduced bone mineral density compromises mechanical strength and increases the risk of screw pull-out. Therefore, rigid locking plates are generally preferred for osteoporotic fracture fixation.[22]

In pediatric patients, retained or even removed implants have been associated with refractures following plate osteosynthesis.[23] These findings suggest that metallic implants may be excessively rigid compared to pediatric bone, thereby contributing to stress shielding. Furthermore, in growing children, retained implants may lead to growth arrest or angular deformities regardless of whether they cross the physis.[24] Moreover, implant retention has been linked to late-onset deep infections and the so-called cutback phenomenon.[25] In contrast to metallic implants, biocomposite materials exhibit lower Young's modulus values, which more closely approximate those of natural bone. This reduces the strain mismatch between the implant and bone, thereby mitigating stress shielding risk. Given their biodegradable nature and potential for osteointegration, these materials may help prevent physeal disruption and eliminate the need for secondary implant removal in pediatric populations.

The mechanical properties of an implant are highly dependent on its design, size, material selection, and postprocessing methods. The literature includes several relevant studies focused on optimizing biocomposite plate designs. One study involving 3D-printed auxetic plates reported improved intraoperative bending flexibility and reduction in stress shielding.[26] A different approach involves combining multiple materials in varied configurations to tailor biomechanical behavior. Fujihara et al.[27] compared braided and knitted carbon fibers integrated into a polyether-ether-ketone matrix, demonstrating that the knitted design achieved 50% higher bending strength but exhibited more deformation under loading compared to the braided variant. In a comparable investigation, researchers developed a fully degradable magnesium fiber reinforced polylactic acid composite and evaluated its structural and mechanical characteristics.[28] One such innovation is the sandwich-type laminated composite, which offers advanced strength and multifunctional characteristics by combining layers of different materials. These sandwich structures allow for the integration of multiple mechanical and chemical advantages within a single implant.[29]

In another study, Chandra et al.[11] developed biodegradable magnesium-based plate models and used FEA to examine the effects of plate thickness, length, and curvature on fracture stability. They identified an optimal plate length of 145 mm and a curvature angle of 130° for magnesium plates.

The bellied and curved designs demonstrated a more complex torsional response. Both geometries reduced plate stress under torsional loading, suggesting that geometric modification can alter stress distribution within the implant. However, the curved model showed higher screw stress, bone stress, and total deformation than the bellied model, indicating that reduced plate stress alone does not necessarily represent superior construct-level torsional performance. The bellied design showed lower torsion-induced deformation and lower plate stress than several other lower-profile composite models, which may reflect a design-related advantage rather than a purely material-volume effect.

The hybrid plate model, which incorporates both flat and curved geometric features, performed better than the metallic plate in the deformation analysis under compressive loading, in contrast to the isolated performance of either design. However, higher bone stress was observed under compressive loading in the hybrid composite model, exceeding those in all other systems. Furthermore, the hybrid model showed high strain responses under compression. Typically, lower strain values are indicative of more rigid and stable constructs with higher load-bearing capacities. The coexistence of minimal total system deformation with higher plate strain likely reflects geometry driven load transfer and stress concentration around bone-screw transitions. Overall, the hybrid model showed the lowest total deformation and implant stress under compression, but its mechanical benefit was load-mode dependent and was not maintained under torsional loading.

The enhanced plate also incorporated elements of both the bellied and curved geometries. It demonstrated relatively low deformation under compression and distraction and showed the lowest plate strain among the composite models under these loading conditions. However, under torsional loading, it showed higher deformation and implant stress than the thick flat and bellied designs. Although the enhanced geometry reduced plate strain and implant stress under axial loading conditions, its structural complexity may require variable screw lengths and may create challenges for soft tissue closure.

Among the flat composite plates, increasing thickness improved construct stiffness and reduced stress, particularly under distraction and torsion. This finding is consistent with the expected contribution of increased cross-sectional inertia. However, the mechanical benefit of the thick flat plate was accompanied by a higher implant profile and greater material volume, which may limit its clinical practicality in regions with limited soft tissue coverage. Another finding was the relatively high bone stress observed under torsional loading. This may be related to the 1 mm fracture gap, which could have limited uniform bone-to-bone contact across the osteotomy during torsion. As a result, stress may have concentrated around the fracture site and screw-bone interface. Although lower peak von Mises stress values may indicate reduced local stress concentration within a given construct, these values should not be interpreted as evidence of implant safety, failure resistance, or cortical bone failure because plasticity, damage, fatigue, and fracture criteria were not included in the present models. Therefore, torsional bone stress values should be interpreted mainly as comparative indicators of load transfer within the present finite element model.

To support the computational credibility of the model in the absence of direct *in vitro* testing, the loading parameters and the baseline mechanical responses were cross-referenced with established biomechanical literature. The compressive load of 800 N applied in our finite element models is directly supported by the experimental *in vitro* testing protocol of Brinkman et al.,[21] who utilized an identical 800 N axial load to simulate full weight-bearing on fourth generation composite femurs following plate fixation. This is also computationally consistent with the 784.8 N loading scenario modeled by Chandra et al.[11] for evaluating biodegradable plates. Furthermore, the mechanical behavioral trend observed in the baseline Ti6Al4V construct, particularly its tendency to exhibit higher implant stress concentrations and lower implant strain than the composite constructs, is in agreement with the comparative FEA findings of Samiezadeh et al.[30] Their study similarly demonstrated that conventional titanium plates absorb the majority of the physiological load, whereas composite plates facilitate a more compliant load-sharing mechanism. Although direct experimental validation was not performed, the computational framework was indirectly supported by comparison with established loading conditions and previously reported finite element trends in the literature. Therefore, the present findings should be interpreted as comparative rather than as experimentally validated predictions.

This study had several limitations. The analyses were performed using an idealized cylindrical

synthetic femoral diaphyseal model rather than patient-specific femoral geometry. Although this approach provided a standardized platform for comparing different plate configurations, it did not fully reproduce the anatomical variability, cortical thickness distribution, medullary morphology, or regional material heterogeneity of the human femur. Bone, metallic implants, and composite implants were modeled as homogeneous, isotropic, and linearly elastic materials; therefore, nonlinear material behavior, plastic deformation, damage accumulation, and failure mechanisms were not evaluated. Second, the screw geometry was simplified by omitting detailed thread morphology, and the screw-bone and plate-screw interfaces were represented using simplified contact assumptions. As a result, thread-dependent parameters such as insertion torque, pull-out strength, and local bone damage around the screw threads could not be assessed. Muscle forces, ligamentous constraints, joint reaction forces, and time-dependent physiological loading were not incorporated. Therefore, the applied compression, distraction, and torsional loads represent simplified loading conditions intended for comparative mechanical evaluation rather than complete simulation of *in vivo* fracture fixation mechanics. Third, in some loading conditions, localized peak stress values exceeded the reported strength range of the corresponding implant material. Since the models did not include plasticity, damage evolution, fatigue, or fracture criteria, these values were not interpreted as definitive implant failure predictions. The primary objective was to evaluate how implant design influenced deformation, stress distribution, and strain patterns under standardized loading conditions, rather than to determine material failure thresholds. Moreover, these loading scenarios should not be interpreted as routine early postoperative loading conditions, since weight-bearing and high-torque activities are typically restricted after plate osteosynthesis. Fourth, the titanium and composite constructs differed not only in material properties but also in implant geometry and screw dimensions, which may have influenced the observed differences in deformation, stress, and strain. Although the titanium reference plate was used for numerical verification of the modelling framework, the individual composite plate configurations were not experimentally validated as manufactured prototypes. Future biomechanical testing will be necessary to confirm the mechanical behavior of the proposed composite designs. Finally, the present analysis did not include cyclic loading, implant degradation, progressive fracture healing, callus formation, or long-term changes in load sharing between the implant and bone. These factors are particularly relevant for biodegradable composite implants and should be addressed in future experimental and computational studies. Consequently, the findings of this study should be interpreted as early-stage finite element predictions that identify design-dependent mechanical trends and guide further prototype development rather than as direct evidence of clinical performance.

In conclusion, implant geometry substantially influenced the mechanical response of biodegradable composite plate constructs, with the hybrid, enhanced, thick flat, and bellied configurations showing load-mode–dependent differences in deformation, implant stress, and strain distribution under compression, distraction, and torsion. These findings support geometry-specific optimization of biodegradable fixation plates as an early design-screening step; however, prototype manufacturing and biomechanical testing are required before any clinical inference can be made.

Data Sharing Statement: The data that support the findings of this study are available from the corresponding author upon reasonable request.

Author Contributions: M.B.A.: Was responsible for the conception and design of the study and performed the data analysis; A.C.T.: Critically evaluated the manuscript and contributed to its intellectual content; S.E.B.: Participated in the study design, data analysis, and interpretation of the results; S.G.: Contributed to data collection; M.K.B.: Assisted in drafting the initial manuscript; E.A.T.: Performed the final review and made editorial revisions to the manuscript. All authors reviewed and approved the final version of the manuscript for submission.

Conflict of Interest: The authors declared no conflicts of interest with respect to the authorship and/or publication of this article.

Funding: The authors received no financial support for the research and/or authorship of this article.

AI Disclosure: The authors declare that artificial intelligence (AI) tools were not used, or were used solely for language editing, and had no role in data analysis, interpretation, or the formulation of conclusions. All scientific content, data interpretation, and conclusions are the sole responsibility of the authors. The authors further confirm that AI tools were not used to generate, fabricate, or 'hallucinate' references, and that all references have been carefully verified for accuracy.

REFERENCES

1. Kandemir U, Augat P, Konowalczyk S, Wipf F, von Oldenburg G, Schmidt U. Implant material, type of fixation at the shaft, and position of plate modify biomechanics of distal femur plate osteosynthesis. J Orthop Trauma 2017;31:e241-6. doi: 10.1097/BOT.0000000000000860.

2. Mehboob H, Chang SH. Optimal design of a functionally graded biodegradable composite bone plate by using the Taguchi method and finite element analysis. Compos Struct 2015;119:166-73. doi: 10.1016/j.compstruct.2014.08.029.
3. Mehboob A, Mehboob H, Chang SH, Tarlochan F. Effect of composite intramedullary nails (IM) on healing of long bone fractures by means of reamed and unreamed methods. Compos Struct 2017;167:76-87. doi: 10.1016/j.compstruct.2017.01.076.
4. Wee H, Staub J, Koroneos Z, Kunselman A, Reid JS, Lewis GS. Mechanics of dynamic compression plate application in fracture fixation. Clin Biomech (Bristol) 2024;113:106209. doi: 10.1016/j.clinbiomech.2024.106209.
5. Claes L. Biomechanical principles and mechanobiologic aspects of flexible and locked plating. J Orthop Trauma 2011;25:S4-7. doi: 10.1097/BOT.0b013e318207093e.
6. Chmielewska A, Dean D. The role of stiffness-matching in avoiding stress shielding-induced bone loss and stress concentration-induced skeletal reconstruction device failure. Acta Biomater 2024;173:51-65. doi: 10.1016/j.actbio.2023.11.011.
7. Bradley GW, McKenna GB, Dunn HK, Daniels AU, Statton WO. Effects of flexural rigidity of plates on bone healing. J Bone Joint Surg Am 1979;61:866-72.
8. Ramakrishna S, Mayer J, Wintermantel E, Leong KW. Biomedical applications of polymer-composite materials: a review. Compos Sci Technol 2001;61:1189-224. doi: 10.1016/S0266-3538(00)00241-4.
9. Lopez J, Siegel N, Reategui A, Faateh M, Manson PN, Redett RJ. Absorbable fixation devices for pediatric craniomaxillofacial trauma: A systematic review of the literature. Plast Reconstr Surg 2019;144:685-92. doi: 10.1097/PRS.0000000000005932.
10. Xiong Y, Ren C, Zhang B, Yang H, Lang Y, Min L, et al. Analyzing the behavior of a porous nano-hydroxyapatite/polyamide 66 (n-HA/PA66) composite for healing of bone defects. Int J Nanomedicine 2014;9:485-94. doi: 10.2147/IJN.S52990.
11. Chandra G, Pandey A, Pandey S. Design of a biodegradable plate for femoral shaft fracture fixation. Med Eng Phys 2020;81:86-96. doi: 10.1016/j.medengphy.2020.05.010.
12. ASTM F136-12. Standard Specification for Wrought Titanium-6Aluminum-4Vanadium ELI (Extra Low Interstitial) Alloy for Surgical Implant Applications (UNS R56401). 2012. doi: 10.1520/F0136-12.
13. Li K, Tjong SC. Mechanical, thermal and bioactive behaviors of polyamide 6/hydroxyapatite nanocomposites. J Nanosci Nanotechnol 2011;11:10644-8. doi: 10.1166/jnn.2011.3955.
14. Zdero R, Brzozowski P, Schemitsch EH. Biomechanical properties of artificial bones made by Sawbones: A review. Med Eng Phys 2023;118:104017. doi: 10.1016/j.medengphy.2023.104017.
15. ASTM International. ASTM F382-17. Standard Specification and Test Method for Metallic Bone Plates. West Conshohocken (PA): ASTM International; 2017. doi: 10.1520/F0382-17.
16. Uhthoff HK, Poitras P, Backman DS. Internal plate fixation of fractures: Short history and recent developments. J Orthop Sci 2006;11:118-26. doi: 10.1007/s00776-005-0984-7.
17. ASTM International. ASTM F543-13E01. Standard Specification and Test Methods for Metallic Medical Bone Screws. West Conshohocken (PA): ASTM International; 2013. doi:10.1520/F0543-13E01.
18. Oefner C, Herrmann S, Kebbach M, Lange HE, Kluess D, Woiczinski M. Reporting checklist for verification and validation of finite element analysis in orthopedic and trauma biomechanics. Med Eng Phys 2021;92:25-32. doi: 10.1016/j.medengphy.2021.03.011.
19. Moazen M, Mak JH, Jones AC, Jin Z, Wilcox RK, Tsiridis E. Evaluation of a new approach for modelling the screw-bone interface in a locking plate fixation: A corroboration study. Proc Inst Mech Eng H 2013;227:746-56. doi: 10.1177/0954411913483259.
20. Biemond JE, Aquarius R, Verdonschot N, Buma P. Frictional and bone ingrowth properties of engineered surface topographies produced by electron beam technology. Arch Orthop Trauma Surg 2011;131:711-8. doi: 10.1007/s00402-010-1218-9.
21. Brinkman JM, Hurschler C, Agneskirchner J, Lobenhoffer P, Castelein RM, van Heerwaarden RJ. Biomechanical testing of distal femur osteotomy plate fixation techniques: The role of simulated physiological loading. J Exp Orthop 2014;1:1. doi: 10.1186/s40634-014-0001-1.
22. Osterhoff G, Morgan EF, Shefelbine SJ, Karim L, McNamara LM, Augat P. Bone mechanical properties and changes with osteoporosis. Injury 2016;47:S11-20. doi: 10.1016/S0020-1383(16)47003-8.
23. Montgomery BK, Gamble JG, Kha ST, Hecht GG, Vorhies JS, Lucas JF. Indications for and risks associated with implant removal after pediatric trauma. J Am Acad Orthop Surg Glob Res Rev 2022;6:e22.00050. doi: 10.5435/JAAOSGlobal-D-22-00050.
24. May C, Yen YM, Nasreddine AY, Hedequist D, Hresko MT, Heyworth BE. Complications of plate fixation of femoral shaft fractures in children and adolescents. J Child Orthop 2013;7:235-43. doi: 10.1007/s11832-013-0496-5.
25. Gamble JG, Ziino C, Imrie MN, Young JL. Trans-metaphyseal screws placed in children: An argument for monitoring and potentially removing the implants. J Pediatr Orthop 2019;39:e28-31. doi: 10.1097/BPO.0000000000001280.
26. Vijayavenkataraman S, Gopinath A, Lu WF. A new design of 3D-printed orthopedic bone plates with auxetic structures to mitigate stress shielding and improve intra-operative bending. Bio-des Manuf 2020;3:98-108. doi: 10.1007/s42242-020-00066-8.
27. Fujihara K, Huang ZM, Ramakrishna S, Satknanantham K, Hamada H. Feasibility of knitted carbon/PEEK composites for orthopedic bone plates. Biomaterials 2004;25:3877-85. doi: 10.1016/j.biomaterials.2003.10.050.
28. Li X, Chu C, Zhou L, Bai J, Guo C, Xue F, et al. Fully degradable PLA-based composite reinforced with 2D-braided Mg wires for orthopedic implants. Compos Sci Technol 2017;142:180-8. doi: 10.1016/j.compscitech.2017.02.013.
29. Arumugam S, Kandasamy J, Md Shah AU, Hameed Sultan MT, Safri SNA, Abdul Majid MS, et al. Investigations on the mechanical properties of glass fiber/sisal fiber/chitosan reinforced hybrid polymer sandwich composite scaffolds for bone fracture fixation applications. Polymers (Basel) 2020;12:1501. doi: 10.3390/polym12071501.
30. Samiezadeh S, Tavakkoli Avval P, Fawaz Z, Bougherara H. On optimization of a composite bone plate using the selective stress shielding approach. J Mech Behav Biomed Mater 2015;42:138-53. doi: 10.1016/j.jmbbm.2014.11.015.